

North Pacific Gyre Oscillation Synchronizes Climate Fluctuations in the Eastern and Western Boundary Systems*

LINA I. CEBALLOS, EMANUELE DI LORENZO, AND CARLOS D. HOYOS

School of Earth and Atmospheric Sciences, Georgia Institute of Technology, Atlanta, Georgia

NIKLAS SCHNEIDER

International Pacific Research Center, University of Hawaii at Manoa, Honolulu, Hawaii

BUNMEI TAGUCHI

Earth Simulator Center, Japan Agency for Marine-Earth Science and Technology, Yokohama, Japan

(Manuscript received 19 September 2008, in final form 23 February 2009)

ABSTRACT

Recent studies have identified the North Pacific Gyre Oscillation (NPGO) as a mode of climate variability that is linked to previously unexplained fluctuations of salinity, nutrient, and chlorophyll in the northeast Pacific. The NPGO reflects changes in strength of the central and eastern branches of the subtropical gyre and is driven by the atmosphere through the North Pacific Oscillation (NPO), the second dominant mode of sea level pressure variability in the North Pacific. It is shown that Rossby wave dynamics excited by the NPO propagate the NPGO signature in the sea surface height (SSH) field from the central North Pacific into the Kuroshio–Oyashio Extension (KOE), and trigger changes in the strength of the KOE with a lag of 2–3 yr. This suggests that the NPGO index can be used to track changes in the entire northern branch of the North Pacific subtropical gyre. These results also provide a physical mechanism to explain coherent decadal climate variations and ecosystem changes between the North Pacific eastern and western boundaries.

1. Introduction

Decadal time-scale climate variability in the North Pacific has received considerable attention in the recent years because of its impact on tropical and extratropical climate (e.g., Deser et al. 1999; Graham 1994), weather over North America (e.g., Latif and Barnett 1994; Barlow et al. 2001), and regional marine ecosystems (e.g., Mantua et al. 1997; Francis et al. 1998; Fiedler 2002). Analyses of sea level pressure (SLP) data suggest that there are two dominant modes of atmospheric variability in the North Pacific. The first one (Fig. 1a) is associated with changes in the Aleutian low and its temporal evolution is called the North Pacific index

(NPI; e.g., Trenberth and Hurrell 1994). The second one is termed the North Pacific Oscillation (NPO; Walker and Bliss 1932; Rogers 1981; Linkin and Nigam 2008).

In the central North Pacific, a strengthened Aleutian low is associated with a decrease of sea surface temperature (SST) as a result of cold air advection from the north, an increase of ocean–atmosphere turbulent heat fluxes, and equatorward advection of temperature from Ekman currents. In the eastern North Pacific, a deepened Aleutian low intensifies poleward winds, leading to warm SST anomalies along the west coast of North America, the Gulf of Alaska, and across the eastern subtropics and tropics (Schneider and Cornuelle 2005). Changes in the Aleutian low also affect the western Pacific because anomalous wind stress curl in the central Pacific force the circulation to change and baroclinic Rossby waves to propagate from the central North Pacific to the western boundary, arriving several years after the Aleutian low changes, resulting in a lagged SST response in the Kuroshio–Oyashio Extension (KOE) region (Miller et al. 2004). The pattern of SST anomalies

* International Pacific Research Center Contribution Number 590.

Corresponding author address: Lina I. Ceballos, 311 Ferst Drive, School of Earth and Atmospheric Sciences, Georgia Institute of Technology, Atlanta, GA 30332-0340.
E-mail: lina.cebillos@eas.gatech.edu

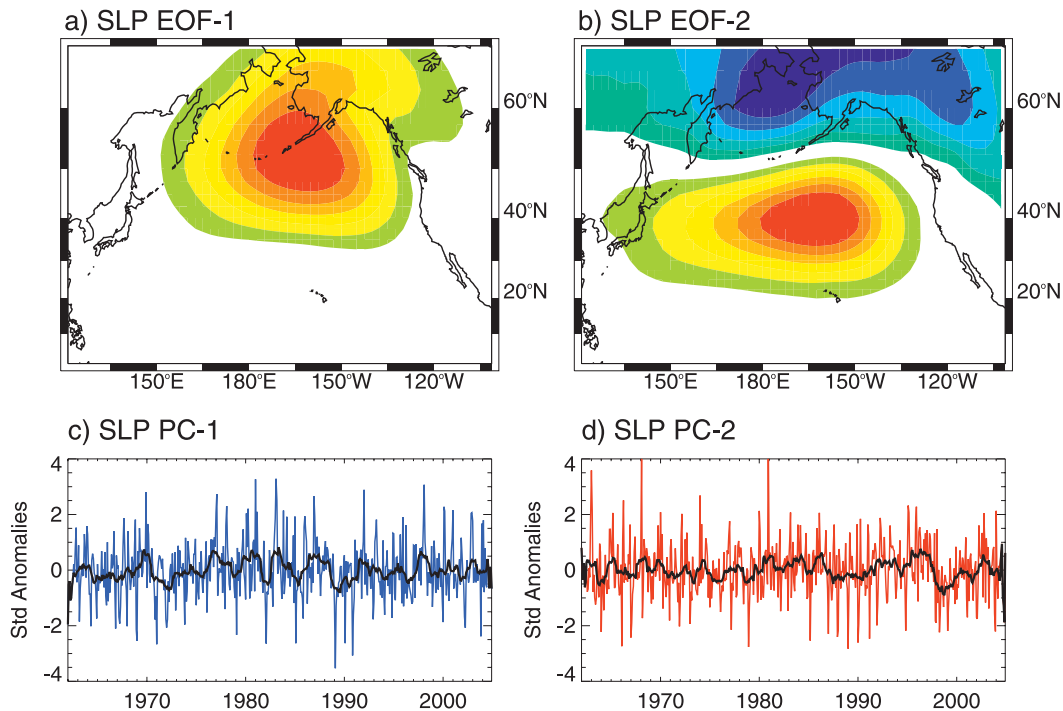


FIG. 1. (a) EOF1 and (b) EOF2 of monthly sea level pressure anomalies during 1950–2004 over the North Pacific and its associated (c) PC-1 and (d) PC-2. The EOFs explain 32.5% and 18.7% of the total SLP variance. In (c), (d), the thick black lines represent a 12-month running mean.

associated to the Aleutian low variability is consistent with the spatial pattern of the Pacific decadal oscillation (PDO; Mantua et al. 1997) defined as the leading empirical orthogonal function (EOF) of SST anomalies in the Pacific, north of 20°N. This pattern similarity has led to studies linking PDO to changes in the atmospheric SLP following the earlier study of Davis (1976). Using the first-order autoregressive (AR-1) model processes, Schneider and Cornuelle (2005) and Chhak et al. (2009) found that SLP anomalies in the Aleutian low had high skill in reconstructing the observed PDO amplitude.

In contrast to the Aleutian low mode, the NPO spatial pattern consists of a dipole structure in which SLP variations in the central Pacific near 40°N oppose those over Alaska (Fig. 1b). Walker and Bliss (1932) found significant correlation between the NPO and precipitation and surface air temperature anomalies over North America and Asia. Rogers (1981) linked the NPO with the advance and retreat of the sea ice edge in the Bering Sea. Chiang and Vimont (2004) linked the NPO with the Pacific meridional mode and with the forcing of El Niño–Southern Oscillation (ENSO) via the SST footprint mechanism (Vimont et al. 2001, 2003). Recently, Chhak et al. (2009) found that the NPO has an oceanic expression termed the North Pacific Gyre Oscillation (NPGO; Di Lorenzo et al. 2008), which is evident from

an analysis of sea surface height anomalies (SSHAs) in the northeast Pacific. The NPGO mode, defined as the EOF/principal component (PC)-2 of SSHa over the region of 25°–62°N, 180°–110°W, is independent from the PDO ($R = 0.15$) and is characterized by a dipole structure in SSHa. This NPGO dipole structure is evident in the high-resolution ocean model hindcast of the OGCM for the Earth Simulator (OFES; discussed in section 2) over the period of 1950–2004 (Fig. 2a). Physically the NPGO reflects variations in the strength of the eastern and central branches of the subpolar and subtropical gyres, as is shown in Fig. 2b, where the red curve corresponds to the NPGO index (PC-2 of SSHa) and the black curve is a measure of the strength of North Pacific Current (Fig. 2a, black box), which is inferred by taking the SSHa meridional gradient in the region marked by the black rectangle in Fig. 2a. Di Lorenzo et al. (2008) showed that previously unexplained fluctuations of salinity, nutrient, and chlorophyll observed in the northeast Pacific track the NPGO index.

In this work, we explore the relationship between decadal variations in the eastern and western boundary current systems of the North Pacific Ocean. Specifically, we show how NPGO variability in the central and eastern North Pacific is connected to decadal variations in the KOE with a phase lag of approximately 2–3 yr. We

a) Correlation NPGO - OFES SSHa

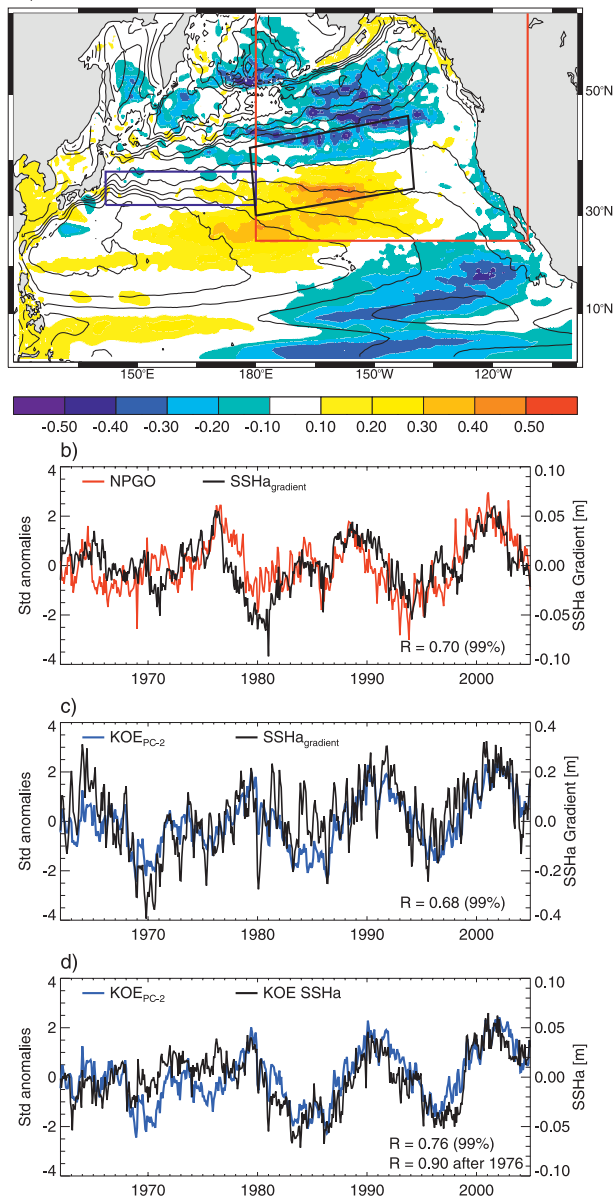


FIG. 2. (a) Correlation map between the NPGO index and the OFES SSHa in the North Pacific (shaded contours). The red box delimits the region where the NPGO index is defined. The contour lines represent the mean sea level. (b) Time series of the NPGO index (red line) and the SSHa gradient (black box). This gradient represents the strength of the central/eastern branches of the subpolar and subtropical gyres. (c) Time series of the second mode of variability in the KOE (blue curve) and the SSHa gradient in the KOE region (black box), which corresponds to the strength of the Kuroshio Extension jet.

explore this connection using both a statistical and a dynamical approach. The statistical approach involves time-lagged spatial correlation maps that show how the NPGO SSHa pattern propagates westward in the KOE,

where it tracks decadal variations in the strength of the KOE and of the average SSHa. The dynamical approach explores the east–west relationship using a simple linear Rossby wave model. The role of Rossby wave dynamics in explaining climate variability of the KOE has been pointed out in several studies (e.g., Kwon and Deser 2007; Qiu 2003; Schneider et al. 2002; Seager et al. 2001). Using a reduced-gravity model, Qiu (2003) tracked the baroclinic oceanic response back to surface winds and showed that variability on the Kuroshio Extension is remotely forced by wind stress anomalies in the eastern/central North Pacific. We follow Qiu’s methodology to explore whether the NPO—the forcing of the NPGO—modulates SSHa variability on the western boundary. To do this we decompose the wind stress in two components: one associated with the Aleutian low mode and one related with the NPO. This allows us to assess the relative contribution of the two dominant atmospheric forcing modes on SSHa variability in the KOE. We also use SSH data from satellite [Archiving, Validation, and Interpretation of Satellite Oceanographic data (AVISO); information online at <http://www.jason.oceanobs.com>] and from a high-resolution eddy-resolving model hindcast of the Earth Simulator (Masumoto et al. 2004; Sasaki et al. 2008). The OFES model captures the decadal variations in the KOE realistically (Taguchi et al. 2007), as well as the NPGO pattern (see Fig. 2a; the regression map between OFES SSHa and the NPGO index is taken from <http://ocean.eas.gatech.edu/npgo>).

This article is organized as follows. Section 2 describes the observational and modeling datasets used in this study. Section 3 examines the statistical relationship between the NPGO and low-frequency variability in the KOE using the OFES model hindcast. Section 4 shows the results from the Rossby wave model and a comparison with SSHa from satellite and OFES. Discussions and conclusions are given in section 5.

2. Data

Monthly sea surface height fields from a hindcast by the OFES (Masumoto et al. 2004; Sasaki et al. 2008) are used in this study. The model extends from 75°S to 75°N, with a horizontal resolution of 0.1° and 54 vertical levels, spanning the period of 1950–2004. In this study, we analyze data from the 1962–2004 period (as in Taguchi et al. 2007). The OGCM was forced by surface wind stress, heat, and freshwater fluxes derived from daily National Centers for Environmental Prediction–National Center for Atmospheric Research (NCEP–NCAR) reanalysis (Kalnay et al. 1996), and there is a relaxation of surface salinity to the observed climatology. The model hindcast has been successfully

used in previous studies to analyze different aspects of the decadal variability in the KOE (Nonaka et al. 2006; Taguchi et al. 2007). In particular, the observed southward shift and the intensification of the Kuroshio and Oyashio jets after the 1976/77 climate shift of the North Pacific were detectable on the OFES output (Nonaka et al. 2006).

Surface wind stress from the NCEP–NCAR reanalysis is used to represent the atmospheric forcing field. This dataset has a spatial resolution of 1.9° latitude \times 1.875° longitude and covers the same time period as the OFES integration. Sea level pressure from NCEP–NCAR reanalysis with a 2.5° spatial resolution is also used to determine the principal modes of North Pacific atmospheric variability. Ocean Topography Experiment (TOPEX)/Poseidon altimeter data (Ducet et al. 2000) from 1993 to 2004 are used for comparison with the OFES and the Rossby wave model output.

3. KOE decadal variability

The Kuroshio–Oyashio Extension has been identified in several studies as a region where strong ocean–atmosphere interaction takes place in the North Pacific (Latif and Barnett 1994; Pierce et al. 2001; Schneider et al. 2002; Qiu et al. 2007). It also has been recognized as a region where the ocean circulation is most variable and where the subsurface ocean variability strongly affects sea surface temperature via vertical entrainment (Schneider et al. 2002) or horizontal advection by the Kuroshio and Oyashio jets (Qiu 2000; Seager et al. 2001; Kwon and Deser 2007). The Kuroshio Extension SSH is highly variable on interannual and decadal time scales. An EOF analysis of the zonal mean SSH anomalies averaged between 142°E and 180° within 30° – 45°N identified two dominant modes of SSH variability in the Kuroshio Extension (Taguchi et al. 2007). The first mode corresponds to changes in the mean latitudinal position of the Kuroshio Extension jet and shows the southward shift of the jet since the 1976/77 North Pacific climate shift. The second mode displays quasi-regular oscillations with a period of 10–15 yr (Fig. 2c, blue curve) and represents an intensification of the Kuroshio jet. It tracks the SSH meridional gradient in the latitudinal band of the KE jet core between 34.5° and 37°N very well [Fig. 2c, black curve $R = 0.71$; see Taguchi et al. (2007)]. After 1976/77, when the SSHs show strong low-frequency fluctuations, these two modes of KOE variability are strongly correlated with SSHa. This implies that a positive SSHa corresponds to a shift in axis and intensification of the KOE. However, we note that the second mode is more strongly correlated ($R = 0.9$) with the KOE SSHa after 1976/77 (Fig. 2d).

We find that the quasi-regular decadal oscillations in the strength of the KOE [Taguchi et al.'s (2007) mode 2] and SSHa are strongly coherent with the NPGO index (Fig. 3). This is evident if we lag the time series of KOE mode 2 and NPGO by approximately 3 yr with the NPGO leading the KOE mode (Fig. 3a). The correlation function between KOE mode 2 and NPGO at different lags (Fig. 3b), shows that the maximum correlation (0.56) between the two time series occurs when NPGO leads KOE by 2.5 yr. Similar results are found if we compare the NPGO with the average SSHa in the KOE (Figs. 3c,d). We also note that a maximum negative correlation occurs when the KOE leads the NPGO by approximately 5 yr (Fig. 3b). The oscillatory nature of the correlation function is interesting and may indicate self-sustaining oscillations of the ocean–atmosphere system in this region as suggested by Pierce et al. (2001) and Qiu et al. (2007). However, in this study we limit our focus only on the dynamics when NPGO is leading.

A lead–lag relationship in the space–time domain reveals that variations in KOE mode 2 are associated with the arrival of NPGO SSHa from the central/eastern Pacific. By performing a time-lagged regression of the OFES North Pacific SSHa with the KOE mode-2 index we obtain spatial maps of the SSHa evolution associated with KOE mode-2 index. Figures 4a,b show correlation maps between SSHa and KOE mode 2 at 0- and -2.5 -yr lag (NPGO leading). At lag 0 much of the North Pacific (north of 45°N) is occupied by negative correlations, whereas positive correlations span from the eastern to the western boundary in the KOE latitudinal band. However, 2.5 yr before (Fig. 4b) negative correlations extended from the eastern to the western boundary, including the KOE latitudinal band, opposing positive correlations south of the Kuroshio region in a pattern that resembles the projection of the NPGO onto the SSHa (Fig. 4c). The similitude between these correlation maps (pattern correlation coefficient = 0.75) indicates again that NPGO leads SSHa variability in the western boundary of the North Pacific, particularly the one associated with the KOE.

Lagged regression maps computed using the monthly anomaly data (not shown) suggest that KOE-related SSH anomalies propagate from the eastern to the western boundary. A time–longitude plot of the lagged correlation maps at 35.25°N (Fig. 4d) shows a propagation of anomalies from the eastern basin into the western North Pacific confirming the east–west phase relationship and suggesting that ocean dynamics may be involved in carrying the NPGO signal from the east into the west. In the next section we will explore this relationship in a dynamical framework to determine

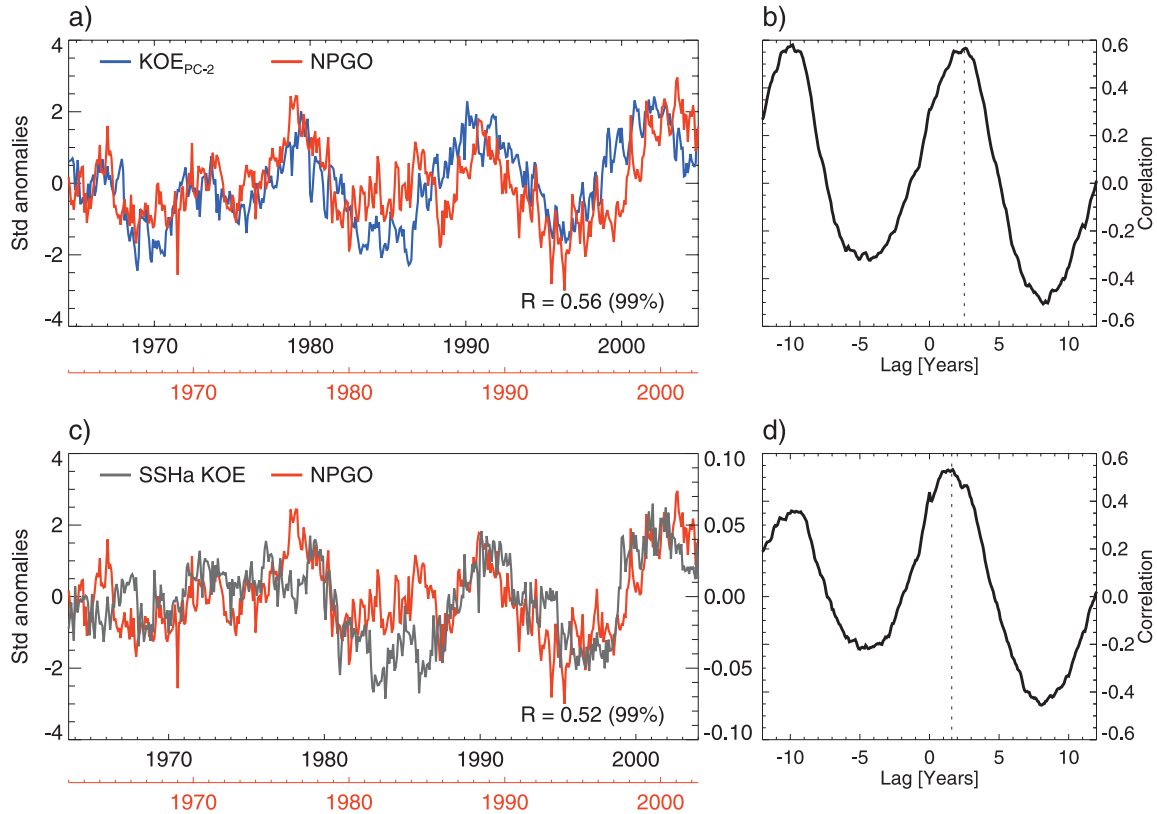


FIG. 3. (a),(c) NPGO (red), KOE mode 2 (blue), and KOE SSHa (gray). The NPGO time axis is shifted (a) 2.5 and (c) 1.5 yr forward in time to match the time of the maximum correlation coefficient (b) between NPGO and KOE mode 2 and (d) between NPGO and KOE SSHa. Positive lag corresponds to NPGO leading and negative lag indicates that NPGO is lagging.

whether the low-frequency variability of SSHa in the western boundary and the NPGO share the same atmospheric forcing, namely, the NPO.

4. Dynamics and processes

On decadal time scales, the subsurface thermocline responds to changes at the surface Ekman pumping, that is, changes of the wind stress curl. In the central North Pacific, anomalies of Ekman pumping associated with the Aleutian low variability excite Rossby waves of the first baroclinic mode that propagates to the western boundary producing the observed decadal variability in the KOE (Deser et al. 1999; Miller et al. 1998; Seager et al. 2001; Kwon and Deser 2007). The concept of linear Rossby waves has been used widely to explain the oceanic response in the KOE to changes in the wind stress in the central Pacific. Using a simplified Rossby wave model, Schneider and Miller (2001) successfully hindcast decadal anomalies of the thermocline depth and use it to predict KOE SST anomalies. Qiu (2003) used the same model to hindcast the SSHa field for the midlatitude North Pacific

and found that the model was able to reproduce the low-frequency SSHa variability in the KE region.

Assuming a $1\frac{1}{2}$ -layer reduced-gravity model, under the longwave approximation, the linear vorticity equation is

$$\frac{\partial h}{\partial t} - c_R \frac{\partial h}{\partial x} = -\frac{g'}{g} w_e, \quad (1)$$

where h is the SSH of interest, c_R is the zonal phase speed of the long baroclinic Rossby wave, g is gravity, g' is the reduced gravity, $w_e = \text{curl}(\tau/f\rho_0)$ is the Ekman pumping velocity, ρ_0 is the density, f is the Coriolis parameter, and τ is the wind stress vector. A detailed derivation of this equation and its solution is presented by Qiu (2002). Integrating Eq. (1) along the baroclinic Rossby wave characteristic and ignoring the SSHa signal from the eastern boundary, we obtain

$$h(x, t) = \frac{g'}{c_R \rho_0 g f} \int_0^x w_e \left(x', t + \frac{x - x'}{c_R} \right) dx'. \quad (2)$$

To hindcast $h(x, t)$ using Eq. (2), monthly wind stress anomalies from NCEP–NCAR reanalysis were used to

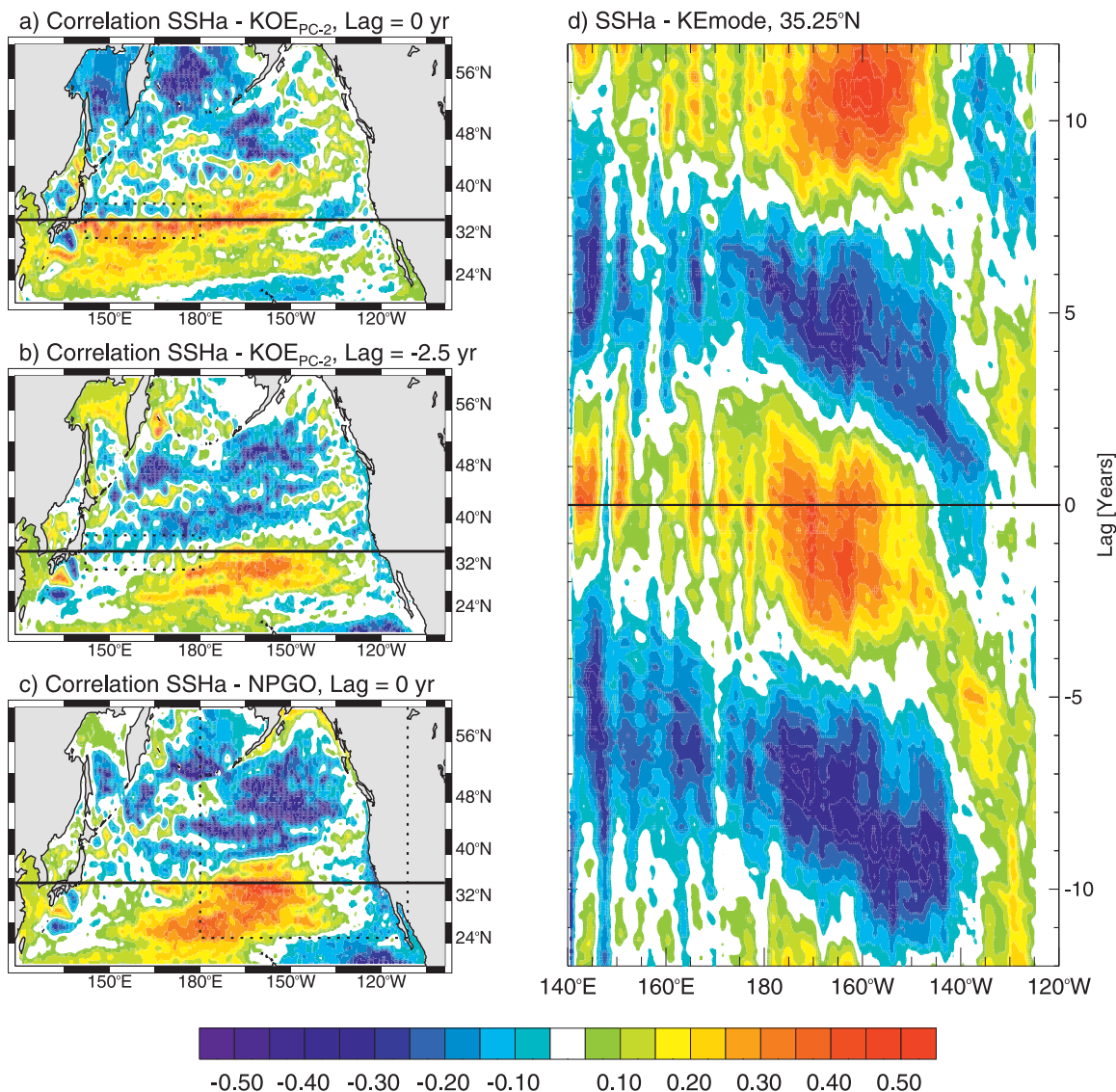


FIG. 4. Spatial correlation pattern between (a) KOE mode 2 and OFES SSHa at 0-yr lag and (b) at lag -2.5 yr (NPGO leading). (c) Spatial correlation between NPGO and SSH anomalies at lag 0. (d) Time-longitude section at 35.25°N (black line on the left panel) of the lagged correlation maps between KOE mode 2 and SSHa. The black box in (a) and (b) represents the region of the KOE, and the box in (c) corresponds to the region of the NPGO.

compute w_e on the grid of the NCEP-NCAR reanalysis. Because the Rossby wave speed c_R varies with latitude, we use the values reported by Qiu (2003) for each latitude of the wind stress curl grid, that is, from 0.041 m s^{-1} at 32°N to 0.024 m s^{-1} at 38°N . Finally, the reduced-gravity value is $g' = 0.027 \text{ m s}^{-2}$.

Figure 5c shows the hindcast monthly SSH anomalies averaged over the latitudinal band of the KOE (32° – 38°N) as a function of time and longitude. For comparison, the SSH anomalies from OFES and satellite data from AVISO are shown in Figs. 5a,b. In both plots, the western boundary shows low-frequency

SSH anomalies arriving from the east during the entire record in the satellite data and since the early 1980s in the OFES output. This confirms the important role that remotely forced SSH anomalies play in modulating the KOE. As noted by Qiu and Chen (2005), the arrival of positive (negative) SSH anomalies to the KOE region corresponds to the strengthening (weakening) of the KE jet and the recirculation gyre. It is worth noting that the Rossby model only captures SSH anomalies resulting from changes in the wind stress and does not account for other dynamic processes such as instabilities and eddy mean flow interaction present

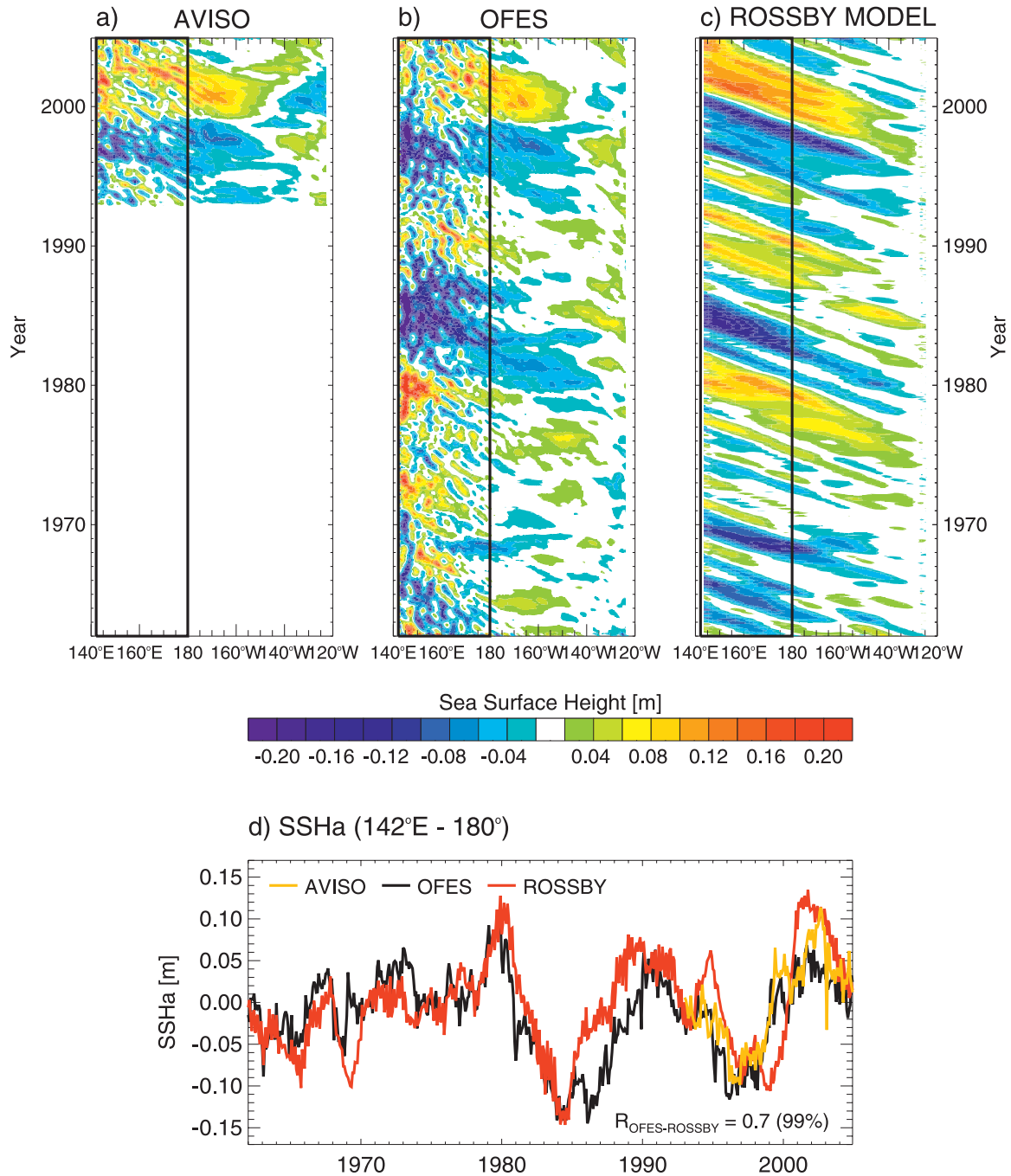


FIG. 5. Time–longitude plots of SSHa averaged between 32.38° and 38.09°N for (a) satellite data, (b) OFES hindcast, and (c) wind stress curl–forced Rossby wave model. (d) The black boxes correspond to the KOE region where (32.38°–38.09°N, 142°E–180°) SSHa was averaged to obtain the time series.

in the KOE region and evident in the OFES data. Also the OFES and satellite data show small-scale high-frequency variability near the western boundary that is not captured by the simple Rossby wave model. However, the Rossby model successfully hindcasts SSH anomalies in the KOE region as shown in Fig. 5d,

which compares time series of mean SSHa between 142°E and 180° from the Rossby model, OFES ($R = 0.7$), and satellite.

Figure 5c also shows that most of the low-frequency SSH signals arriving at the western boundary originate near 150°–160°W in the eastern/central North Pacific,

which is the region where the wind stress curl has its largest amplitude in the North Pacific.

To understand how Pacific decadal oscillations in the eastern North Pacific such as the PDO and the NPGO are linked to the SSH signals in the KOE, we decompose the wind stress curl into the two dominant modes of North Pacific atmospheric variability, the Aleutian low mode, and the NPO mode, which drive the PDO and NPGO, respectively (Chhak et al. 2009). The decomposition was done using a regression analysis between the wind stress curl and each atmospheric mode (PC-1 for the PDO-related wind stress curl and PC-2 for the NPGO case). The regression coefficients were used to reconstruct, separately, the wind stress curl that is then used to force the Rossby model Eq. (2) and hindcast the SSH anomalies in the KOE region. A comparison of SSHa time series in the KOE region shows no correspondence between the SSHa obtained with the Aleutian low forcing and the OFES hindcast (Fig. 6c, top panel). In contrast, the SSHa obtained with the NPO forcing (Fig. 6d, top panel) closely tracks the OFES hindcast ($R = 0.71$) especially after 1976/77 when large-amplitude fluctuations become more apparent. These results indicate that the NPO-related wind stress curl anomalies explains an important fraction of the SSH decadal variability in the KOE. Because the NPO is the forcing pattern of the NPGO in the central and eastern North Pacific (Chhak et al. 2009; Di Lorenzo et al. 2008), this result gives further evidence that SSH variability in the KOE region is dynamically linked to NPGO.

Taguchi et al. (2007) isolate the KOE mode 2 and showed that it is associated with changes in the Kuroshio Extension's strength, but did not provide any forcing mechanism. By linking the NPGO forcing with SSH variability in the KOE we have revealed the forcing of the KOE mode 2 and provided the physical foundation for this mode to exist.

5. Summary and discussion

Using a hindcast experiment by the high-resolution eddy-resolving OFES and sea level pressure, and wind stress curl from the NCEP–NCAR reanalysis, we have studied the relationship between a recently identified mode of decadal variability in the northeast Pacific, the North Pacific Gyre Oscillation (NPGO; Di Lorenzo et al. 2008), and climate variability in the western boundary of the North Pacific. To achieve this goal, we analyzed the low-frequency variability of the SSH anomalies in the Kuroshio–Oyashio Extension region between 32°–38°N and 142°E–180°, which is characterized by two modes of variability. The first mode is associated with changes in the latitudinal position of the

Kuroshio Extension jet, whereas the second one represents variations in the strength of the jet (Taguchi et al. 2007) and displays quasi-decadal oscillations comparable to those of the NPGO index (Fig. 2).

To explore the east–west relationship between the central/eastern North Pacific and the KOE, we used two different approaches. First, we looked for statistical evidence of the link between the NPGO and SSHa variability in the KOE, and second, using a simple linear Rossby wave model, we explored the dynamics underlying the east–west connection. The statistical approach, which involved time-lagged correlations, showed that the NPGO index leads SSHa variability in the KOE by approximately 2–3 yr, which is associated with the strength of the Kuroshio Extension jet. This result is supported by time-lagged spatial correlation maps that show how the NPGO pattern propagates from the eastern/central North Pacific toward the western boundary (Fig. 4), highlighting the role of Rossby waves in carrying the SSHa signature of the NPGO across from the eastern to the western boundary.

Linear baroclinic Rossby wave models have been used to link wind stress curl anomalies in the eastern/central North Pacific with SSHa variability in the Kuroshio Extension (Qiu 2003; Schneider and Miller 2001). The success of these models had led to the hypothesis that Pacific decadal oscillations modulate decadal variability on the western boundary via changes in the wind stress curl field of the eastern/central North Pacific. Here we used a linearized Rossby wave model to hindcast the SSHa in the KOE region and determine to what extent wind stress curl anomalies associated with the forcing of the NPGO, namely the NPO, drive the low-frequency SSHa variability in that region. By decomposing the wind stress curl field into the first two dominant SLP modes of North Pacific variability—the Aleutian low and the NPO mode—we found that the dominant fraction of the KOE SSHa is explained by NPO-related wind stress curl anomalies, whereas the Aleutian low SSH-related anomalies did not compare well with the OFES KOE SSHa (Fig. 6). These results lead us to conclude that the eastern Pacific NPGO and the western Pacific KOE SSHa variability share the same atmospheric forcing, that is, the NPO, and that low-frequency variation the KOE strength are modulated by the NPO.

These results may appear in contrast with previous findings by Qiu (2003), who showed that the westward propagation of positive (negative) SSH anomalies in the KOE are caused by negative (positive) wind stress curl anomalies in the east associated with variability in the PDO rather than NPGO. This difference with Qiu (2003) may be reconciled by noting that Qiu focuses its analysis over a shorter period of 1982–2002. During this

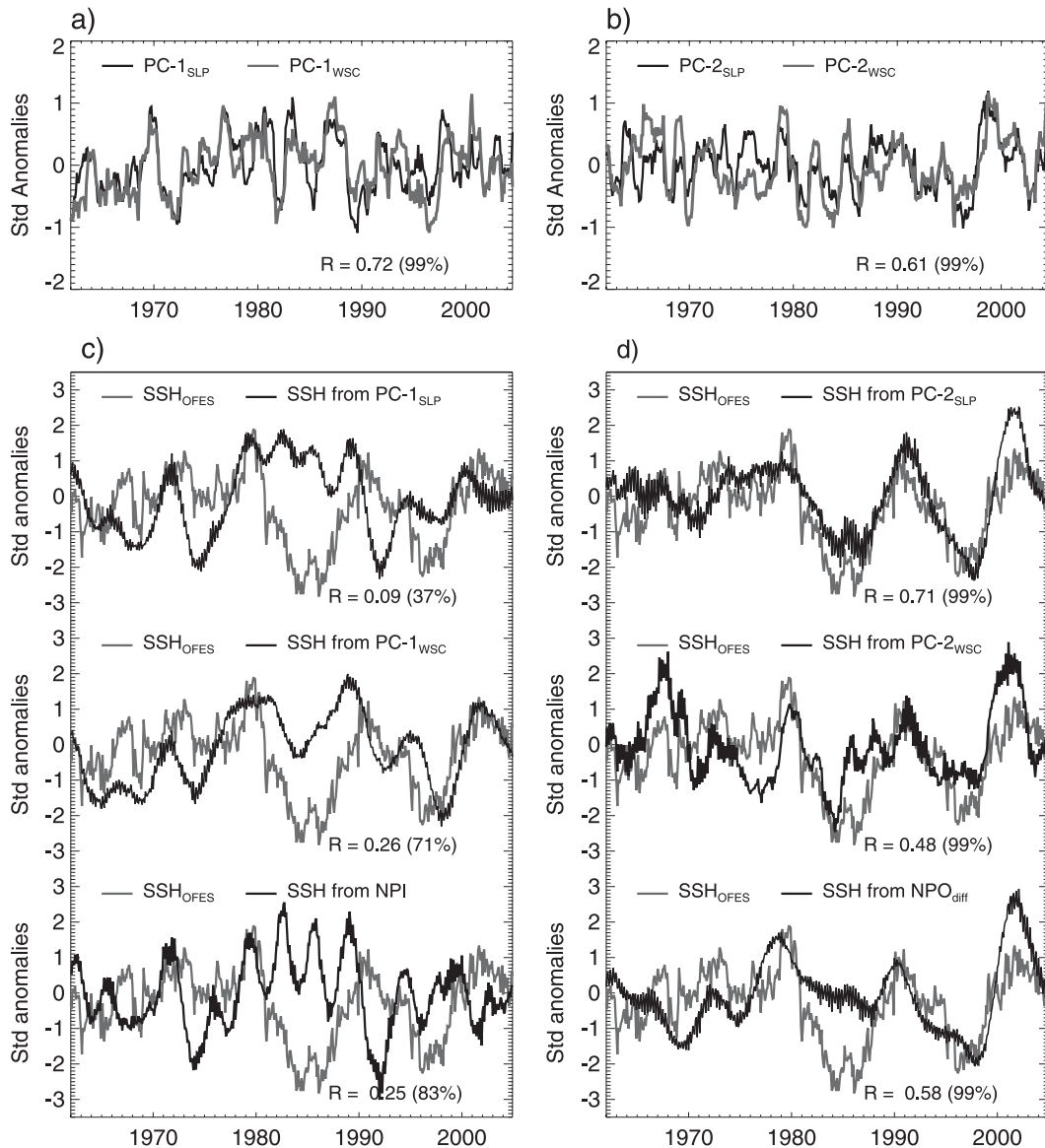


FIG. 6. Comparison between (a) PC-1 of sea level pressure and PC-1 of wind stress curl and PC-2 of sea level pressure and PC-2 of wind stress curl. A 12-month running mean was applied to all the time series. (c)–(d) Time series of SSH a from the Rossby wave model averaged in the KOE region (32.38° – 38.09° N, 142° E– 180°). In all panels the gray curve represents SSHa average from OFES, and the black line corresponds to SSHa from the Rossby model using PC-1 of SLP, PC-1 of wind stress curl, NPI, PC-2 of SLP, PC-2 of wind stress curl, and Chhaks's NPO index as forcing. The time series were standardized for comparison.

time the PDO and NPGO index share some correlation of their low-frequency modulations. This correlation, although not statistically significant, is particularly evident after 1990 ($R = 0.4$), indicating that over this time period it is difficult to separate the relative contributions of PDO and NPGO based on correlation analysis. We also note that Qiu (2003) uses the EOF1 of the wind stress curl anomaly (WSCa) rather than the EOF of the SLP anomaly (SLPa) to characterize the atmospheric driver of the PDO. Although the first EOFs of WSCa

and SLPa are significantly correlated in their low-frequency variability (Figs. 6a,b), their spatial patterns have some important differences in their center of actions (Fig. 7) that lead to changes in the Rossby model hindcast skills (Figs. 6c,d, top panel versus middle panel). We note that the SSHa reconstruction of the Rossby wave model using PC-1 of the WSCa (Fig. 6c, middle panel) exhibits a higher correlation with the KOE SSHa after 1990, consistent with Qiu's findings. However, if we compare the skill of the reconstruction

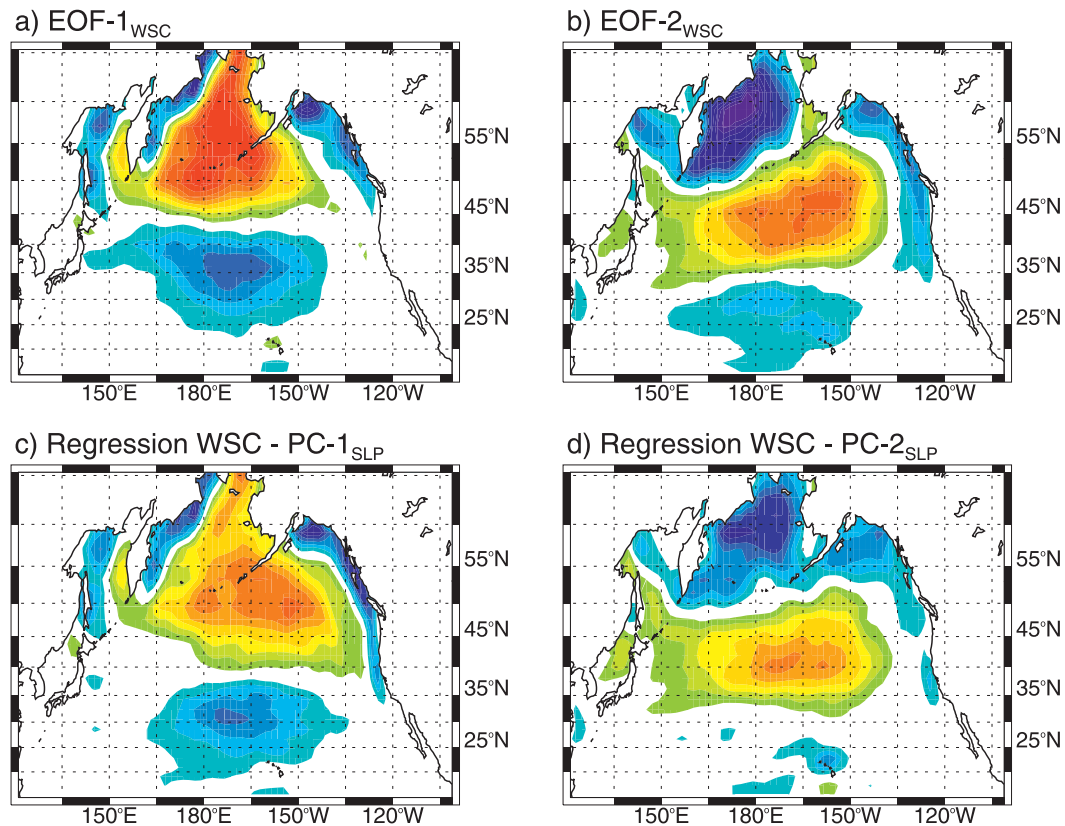


FIG. 7. Wind stress curl anomalies (a) EOF1 and (b) EOF2. Regression map of wind stress curl anomalies vs (c) SLP PC-1 and (d) SLP PC-2.

associated with PC-1 and PC-2 of WSCa over the longer period of 1950–2004, we find that the PC-2 of WSCa leads to higher skill than PC-1 in the SSHa reconstruction (Figs. 6c,d, middle panels). The results obtained with the PCs of the WSCa are consistent with the ones obtained using SLPa and further support the hypothesis that NPO/NPGO variability captured by the second PCs is linked to the dominant SSHa variations in the KOE.

Before concluding we must also remark that the NPO wind stress curl pattern isolated by Chhak et al. (2009) as the forcing of NPGO reveals spatial differences with the NPO pattern inferred as the second EOF of SLP in the North Pacific. These differences reflect the different definitions used for the NPO. In Di Lorenzo et al. (2008) and Chhak et al. (2009), the NPO pattern emerges from a regression of the NPGO index with the atmospheric SLPa, which is equivalent to the second EOF of wind stress curl over the northeast Pacific. In this study we used the more recent definition of NPO by Linkin and Nigam (2008) as the second EOF of North Pacific SLPa. It is important to verify that both definitions of the NPO are consistent with the statement that NPGO is forced by NPO. Using the same approach of Chhak et al. (2009) we use an AR-1 model forced by the NPO indices to

reconstruct the NPGO index. We find that both definitions of the NPO lead to a skillful reconstruction of the NPGO with 99% level significant correlations of 0.48 (NPO defined as the second EOF of SLPa) and 0.71 (NPO defined as the second EOF of wind stress curl in the northeast Pacific). We also verify that using the Chhak et al. (2009) NPO definition as forcing of the Rossby SSHa hindcast model leads to significant skill ($R = 0.58$) in reconstructing the KOE SSHa (Fig. 6d, bottom panel).

Collectively, the results shown in Fig. 6 are consistent with our hypothesis that the NPGO and a significant fraction of SSHa variability in the KOE share the same forcing, namely, the NPO. These results are robust to different definitions of the NPO, which include the PC-2 of SLPa (Linkin and Nigam 2008), PC-2 of WSCa, and the Chhak et al. (2009) index. We also conclude that between 32° and 38°N, low-frequency changes in KOE SSHa are more strongly affected by atmospheric variability associated with the NPO rather than the Aleutian low. To further confirm this statement we perform an additional integration with the Rossby model using the WSCa obtained by regressing the curl anomalies with the NPI index (Trenberth and Hurrell 1994), which is a

measure of the strength of the Aleutian low. The reconstructed SSHa skill using the NPI is very poor compared ($R = 0.25$) to the ones obtained using the various definitions of the NPO ($R = 0.71$, $R = 0.48$, and $R = 0.58$).

Our findings have implications for the predictability of the western North Pacific Ocean climate. Schneider and Miller (2001) showed that wintertime sea surface temperature anomalies in the Kuroshio–Oyashio could be predicted at lead times of up to 2 yr, using the wind stress over the North Pacific and oceanic Rossby wave dynamics. Therefore NPGO–KOE connection may be used to predict western boundary sea surface height fluctuations. Additionally, the results of this study could be extended to determine to what extent, and by what mechanisms, modes of North Pacific variability, such as the NPGO, drive coherent changes in the marine ecosystems of the KOE region.

Acknowledgments. Ceballos and Di Lorenzo acknowledge the support by the National Science Foundation through Grants NSF GLOBEC OCE-0815280, NSF OCE-0550266, NSF GLOBEC OCE-0606575, and NSF CCE-LTER.

Schneider acknowledges the support by the National Science Foundation through Grants NSF OCE05-50233 and NSF OCE06-47994, and by the Office of Science (BER), U.S. Department of Energy, Grant DE-FG02-07ER64469. Additional support was provided by the Japan Agency for Marine–Earth Science and Technology (JAMSTEC), by NASA through Grant NNX07AG53G and by NOAA through Grant NA17RJ1230 through their sponsorship of research activities at the International Pacific Research Center. Taguchi is in part supported by the Agriculture Forestry and Fisheries Research Council of Japan through the research project Population Outbreak of Marine Life (POMAL).

REFERENCES

- Barlow, M., S. Nigam, and E. H. Berbery, 2001: ENSO, Pacific decadal variability, and U.S. summertime precipitation, drought, and stream flow. *J. Climate*, **14**, 2105–2128.
- Chhak, K., E. Di Lorenzo, P. Cummins, and N. Schneider, 2009: Forcing of low-frequency ocean variability in the Northeast Pacific. *J. Climate*, **22**, 1255–1276.
- Chiang, J. C. H., and D. J. Vimont, 2004: Analogous Pacific and Atlantic meridional modes of tropical atmosphere–ocean variability. *J. Climate*, **17**, 4143–4158.
- Davis, R. E., 1976: Predictability of sea surface temperature and sea level pressure anomalies over North Pacific Ocean. *J. Phys. Oceanogr.*, **6**, 249–266.
- Deser, C., M. A. Alexander, and M. S. Timlin, 1999: Evidence for a wind-driven intensification of the Kuroshio Current extension from the 1970s to the 1980s. *J. Climate*, **12**, 1697–1706.
- Di Lorenzo, E., and Coauthors, 2008: North Pacific Gyre Oscillation links ocean climate and ecosystem change. *Geophys. Res. Lett.*, **35**, L08607, doi:10.1029/2007GL032838.
- Ducet, N., P. Y. Le Traon, and G. Reverdin, 2000: Global high-resolution mapping of ocean circulation from TOPEX/Poseidon and ERS-1 and -2. *J. Geophys. Res.*, **105**, 19 477–19 498.
- Fiedler, P. C., 2002: Environmental change in the eastern tropical Pacific Ocean: Review of ENSO and decadal variability. *Mar. Ecol.: Prog. Ser.*, **244**, 265–283.
- Francis, R. C., S. R. Hare, A. B. Hollowed, and W. S. Wooster, 1998: Effects of interdecadal climate variability on the oceanic ecosystems of the NE Pacific. *Fish. Oceanogr.*, **7**, 1–21.
- Graham, N. E., 1994: Decadal-scale climate variability in the tropical and North Pacific during the 1970s and 1980s: Observations and model results. *Climate Dyn.*, **10**, 135–162.
- Kalnay, E., and Coauthors, 1996: The NCEP/NCAR 40-Year Reanalysis Project. *Bull. Amer. Meteor. Soc.*, **77**, 437–471.
- Kwon, Y. O., and C. Deser, 2007: North Pacific decadal variability in the Community Climate System Model version 2. *J. Climate*, **20**, 2416–2433.
- Latif, M., and T. P. Barnett, 1994: Causes of decadal climate variability over the North Pacific and North America. *Science*, **266**, 634–637.
- Linkin, M. E., and S. Nigam, 2008: The North Pacific Oscillation–west Pacific teleconnection pattern: Mature-phase structure and winter impacts. *J. Climate*, **21**, 1979–1997.
- Mantua, N. J., S. R. Hare, Y. Zhang, J. M. Wallace, and R. C. Francis, 1997: A Pacific interdecadal climate oscillation with impacts on salmon production. *Bull. Amer. Meteor. Soc.*, **78**, 1069–1079.
- Masumoto, Y., and Coauthors, 2004: A fifty-year eddy-resolving simulation of the world ocean—Preliminary outcomes of the OFES (OGCM for the Earth Simulator). *J. Earth Simulator*, **1**, 35–56.
- Miller, A. J., D. R. Cayan, and W. B. White, 1998: A westward-intensified decadal change in the North Pacific thermocline and gyre-scale circulation. *J. Climate*, **11**, 3112–3127.
- , F. Chai, S. Chiba, J. R. Moisan, and D. J. Neilson, 2004: Decadal-scale climate and ecosystem interactions in the North Pacific Ocean. *J. Oceanogr.*, **60**, 163–188.
- Nonaka, M., H. Nakamura, Y. Tanimoto, T. Kagimoto, and H. Sasaki, 2006: Decadal variability in the Kuroshio–Oyashio extension simulated in an eddy-resolving OGCM. *J. Climate*, **19**, 1970–1989.
- Pierce, D. W., T. P. Barnett, N. Schneider, R. Saravanan, D. Dommenget, and M. Latif, 2001: The role of ocean dynamics in producing decadal climate variability in the North Pacific. *Climate Dyn.*, **18**, 51–70.
- Qiu, B., 2000: Interannual variability of the Kuroshio extension system and its impact on the wintertime SST field. *J. Phys. Oceanogr.*, **30**, 1486–1502.
- , 2002: Large-scale variability in the midlatitude subtropical and subpolar North Pacific Ocean: Observations and causes. *J. Phys. Oceanogr.*, **32**, 353–375.
- , 2003: Kuroshio extension variability and forcing of the Pacific decadal oscillations: Responses and potential feedback. *J. Phys. Oceanogr.*, **33**, 2465–2482.
- , and S. M. Chen, 2005: Variability of the Kuroshio extension jet, recirculation gyre, and mesoscale eddies on decadal time scales. *J. Phys. Oceanogr.*, **35**, 2090–2103.
- , N. Schneider, and S. M. Chen, 2007: Coupled decadal variability in the North Pacific: An observationally constrained idealized model. *J. Climate*, **20**, 3602–3620.

- Rogers, J. C., 1981: The North Pacific Oscillation. *J. Climatol.*, **1**, 39–58.
- Sasaki, H., M. Nonaka, Y. Masumoto, Y. Sasai, H. Uehara, and H. Sakuma, 2008: An eddy-resolving hindcast simulation of the quasiglobal ocean from 1950 to 2003 on the Earth Simulator. *High Resolution Numerical Modelling of the Atmosphere and Ocean*, K. Hamilton and W. Ohfuchi, Eds., Springer-Verlag, 157–185.
- Schneider, N., and A. J. Miller, 2001: Predicting western North Pacific Ocean climate. *J. Climate*, **14**, 3997–4002.
- , and B. D. Cornuelle, 2005: The forcing of the Pacific decadal oscillation. *J. Climate*, **18**, 4355–4373.
- , A. J. Miller, and D. W. Pierce, 2002: Anatomy of North Pacific decadal variability. *J. Climate*, **15**, 586–605.
- Seager, R., Y. Kushnir, N. H. Naik, M. A. Cane, and J. Miller, 2001: Wind-driven shifts in the latitude of the Kuroshio–Oyashio extension and generation of SST anomalies on decadal timescales. *J. Climate*, **14**, 4249–4265.
- Taguchi, B., S. P. Xie, N. Schneider, M. Nonaka, H. Sasaki, and Y. Sasai, 2007: Decadal variability of the Kuroshio extension: Observations and an eddy-resolving model hindcast. *J. Climate*, **20**, 2357–2377.
- Trenberth, K. E., and J. W. Hurrell, 1994: Decadal atmosphere–ocean variations in the Pacific. *Climate Dyn.*, **9**, 303–319.
- Vimont, D. J., D. S. Battisti, and A. C. Hirst, 2001: Footprinting: A seasonal connection between the tropics and mid-latitudes. *Geophys. Res. Lett.*, **28**, 3923–3926.
- , J. M. Wallace, and D. S. Battisti, 2003: The seasonal footprinting mechanism in the Pacific: Implications for ENSO. *J. Climate*, **16**, 2668–2675.
- Walker, G., and E. Bliss, 1932: World weather V. *Mem. Roy. Meteor. Soc.*, **4**, 53–84.